System Noise Prediction of the DGEN 380 Turbofan Engine

Jeffrey J. Berton*
NASA Glenn Research Center, Cleveland, Ohio 44135

DOI: 10.2514/1.C033616

The DGEN 380 is a small, separate-flow, geared turbofan being promoted for a small twinjet application in the emerging personal light jet market. Smaller, and producing less thrust than other entries in the industry, the engine could be applied to a four to five place twinjet designed to compete in an area currently dominated by propeller-driven airplanes. This paper documents the procedures used to project static noise measurements collected from the engine to flight conditions and the prediction of certification noise of a notional airplane powered by twin DGEN engines. A novel noise model calibration technique and a Monte Carlo uncertainty experiment are emphasized.

Nomenclature

c	=	speed of sound
D	=	directivity distribution function
F	=	Fresnel number
f	=	frequency
G	=	tip-Mach-dependent fan noise term
H	=	spool-speed-dependent shaft noise term
k	=	convective amplification exponent
L	=	noise level
M	=	Mach number
$\dot{m}$	=	mass flow rate
N	=	shaft speed
n	=	jet noise velocity term exponent
O	=	optimization function
p	=	pressure
S	=	spectral distribution function
T	=	temperature
V	=	velocity
w	=	objective function weighting factor
x	=	empirical calibration variable
α	=	jet convection correlation factor
Δ	=	Fresnel number characteristic length
θ	=	polar (yaw) emission angle, zero at inlet
λ	=	wavelength
ρ	=	density
ω	=	jet noise density term exponent

Subscripts

c	=	convective
e	=	effective
f	=	flight
H	=	high-pressure spool
I	=	shielding insertion loss
i	=	one-third-octave band frequency index
L	=	low-pressure spool
r	=	relative

I. Introduction

APPLICANTS seeking noise-type certification for new civil aircraft will often collect acoustic data from static engine tests to help make more accurate predictions of certification noise. Static noise data can be used to calibrate computational models that project noise to flight conditions and analytically mimic the noise certification environment. Early predictions for system noise levels typically are in hand during aircraft development long before flight tests begin. Guidance for using static noise measurements to make system noise predictions is offered by the International Civil Aviation Organization (ICAO) [1]. Computational tools exist to aid this process. Aircraft community noise prediction software lies in a continuum of software hierarchy that trades fidelity versus scope. Tools appropriate for this level of analysis usually consist of empirical to semi-empirical modules that are relatively quick to execute, propagate noise spectra to the ground, and predict single-event community noise metrics. Company-based software in this category is usually proprietary and unpublished; however, known examples of these kinds of computer codes include Boeing's Modular Component Prediction software [2] and the methods distributed by the Engineering Sciences Data Unit [3]. Another is NASA's Aircraft Noise Prediction Program (ANOPP)† [4,5], the software used in this study. The noise modeling technique is applied to a new small turbofan engine not yet adapted to an airplane, with a result interesting to the business jet community.

The DGEN 380 is twin-spool, unboosted, separate-flow, geared turbofan manufactured by Price Induction, Inc. with a static thrust of up to 570 lb at sea level. The design fan pressure ratio is low enough to allow a very high bypass ratio (7.6) for an engine this small. The 14-in.-diam fan is geared, and fan tip speeds are subsonic. The core turbomachinery consists of a radial compressor and high- and low-pressure axial turbines. The inlet and bypass exhaust ducts are hardwall with no acoustic treatment. The engine exhausts through a coannular plug nozzle. A cutaway view of the engine is shown in Fig. 1.

DGEN 380 and 390 series turbofans are being promoted for a small twinjet application in the emerging light jet market. DGEN engines are smaller and produce less thrust than other entries offered, such as the Williams International FJ33 and the Pratt and Whitney PW600 series engines. Nomenclature for these new light jets seems ill defined as of this writing; they are called very light jets by some and personal light jets by others, depending on characteristics such as gross weight, payload, and performance. Available light jets are Eclipse Aviation's 500/550, Cessna's 510 Citation Mustang, and Embraer's Phenom 100, and Honda's HA-420 HondaJet is expected to be fully certified by the time this report is published. Light jet programs under development include Cirrus Aircraft's Vision SF50, and Diamond Aircraft's D-Jet (although the development of the D-Jet has been suspended).

Noise measurements of a DGEN 380 were made in 2015 at NASA Glenn's Aero-Acoustic Propulsion Laboratory. The laboratory is a large dome, 65 ft high and 130 ft in diameter. It is fitted with acoustic

Presented as Paper 2015-2516 at the 21st AIAA/CEAS Aeroacoustics Conference, Dallas, TX, 22–26 June 2015; received 1 July 2015; revision received 11 February 2016; accepted for publication 6 March 2016; published online 25 May 2016.

*Aerospace Engineer, Propulsion Systems Analysis Branch, MS 5-11. Senior Member AIAA.

†Currently maintained at NASA Langley by the ANOPP team in electronic format and provided upon request; latest revision: Level 31.

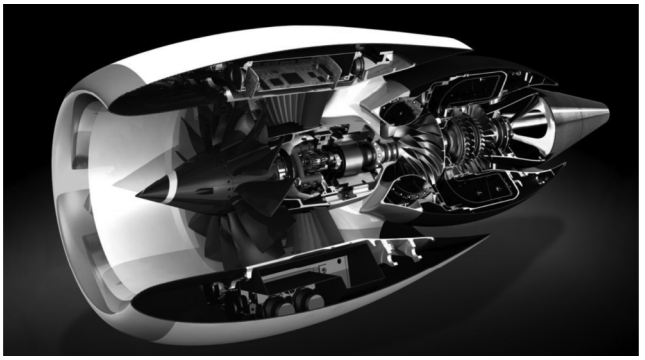

Fig. 1 Cutaway view of the DGEN 380 turbofan.

foam wedges, creating an anechoic environment down to 250 Hz, ideal for acoustic testing. The truck-mounted engine was located under an array of microphones designed for the dome's nozzle acoustic test rig. Photos of the DGEN 380 parked inside the facility are shown in Figs. 2 and 3. An inlet control device designed to reduce inflow distortion can be seen in Fig. 3.

Narrowband acoustic spectra were measured at 24 emission angles (ranging from 36 to 145 deg relative to the inlet axis) and at six engine throttle settings. These measurements are the basis of this investigation. This paper documents the procedures used to project the DGEN static noise measurements to flight conditions and the prediction of system noise of a hypothetical airplane powered by twin DGEN engines. A novel process of calibrating empirical noise models to the measured noise spectra is described. This form of regression allows a model to be calibrated to not only the shape of each experimental spectrum, but also to other derived-noise metrics of importance. This calibration process also enables a Monte Carlo uncertainty experiment (also presented in this paper) to be more easily implemented.

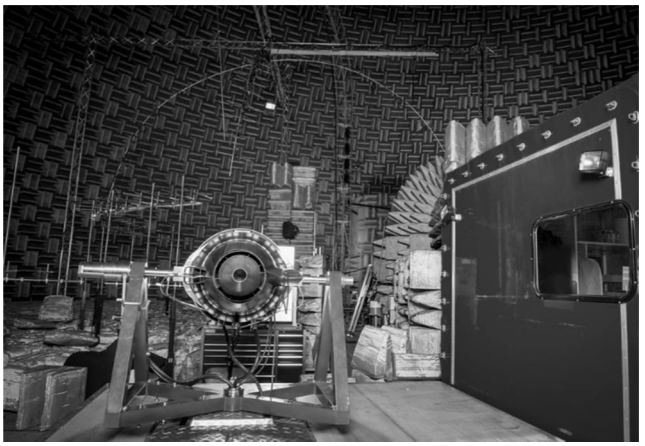

Fig. 2 Rear view of DGEN 380 turbofan inside NASA Glenn Aero-Acoustic Propulsion Laboratory anechoic dome.

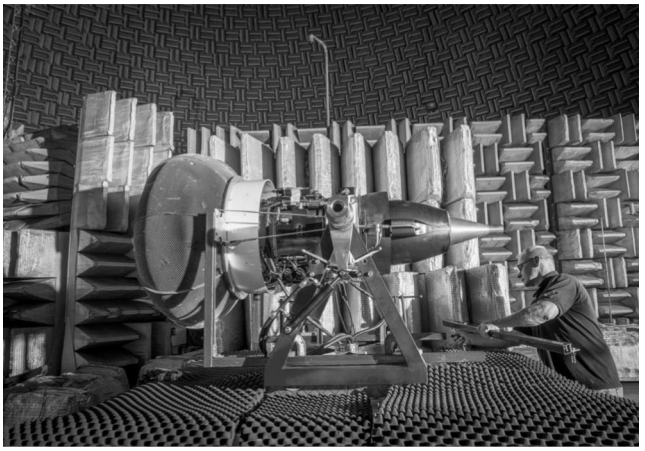

Fig. 3 Portside view of DGEN 380 turbofan, showing installation of inlet control device.

II. Method of Analysis

A concept suggested by Price Induction and shown in their promotional literature is a jet-powered airplane similar to Cirrus Aircraft's propeller-driven SR22. The piston engine and propeller are removed and two DGEN 380 engines are mounted on the fuselage. This notional four-place personal light jet is illustrated in Fig. 4. With a maximum takeoff gross weight of just 3400 lb, a DGEN-powered SR22 variant is representative of the type of general aviation airplane targeted by Price Induction, and it is the airplane analytically modeled in this noise evaluation. Using a hypothetical SR22 variant in this study is not meant to be an endorsement of the concept, nor is it intended to detract from the development of Cirrus Aircraft's actual foray into the personal jet market: the larger seven-place 6000 lb single-engine Vision SF50.

The aircraft system noise metric chosen for this analysis is the effective perceived noise level (EPNL). Under ICAO and Federal Aviation Administration (FAA) noise regulations (ICAO's Annex 16 [6], or its FAA equivalent, Part 36 [7]), any manufacturer seeking a noise-type certificate for a nonexperimental, civilian airplane equipped with DGEN turbofans would need to certify it as a jet-powered subsonic airplane. Despite its small size, and despite that small propeller-driven airplanes in its competitive market normally certify under much simpler noise regulations, a DGEN-powered airplane would be certified under regulations reserved for transport-category large airplanes. Jet-powered airplanes regardless of size are required to certify using the EPNL noise metric and measurement procedures. The limits of the EPNL (i.e., how much noise an airplane is permitted to make) are regulated by ICAO's Annex 16.

EPNLs are computed from acoustic measurements made during a certification test as an airplane flies past three observation monitors on the ground (shown in Fig. 5). The EPNL is a metric sensitive to level, frequency, tone content, and duration of a single airplane flyover event. The cumulative, or algebraic, sum of the three certification EPNLs is often used to capture all three measurements.

The DGEN's noise spectra (measured statically and corrected for atmospheric absorption) can be analytically projected to simulated flight conditions by accounting for convective amplification and Doppler shift effects. Propagation phenomena such as spherical spreading, atmospheric absorption, and various ground effects can also be added to simulate a real airplane flyover event.

A sample noise spectrum acquired from the DGEN turbofan is shown in Fig. 6. Narrowband power spectral densities emitted 118 deg from the inlet axis are plotted. The engine is operating at 96%

Fig. 4 Notional four-place personal light jet powered by twin DGEN 380s.

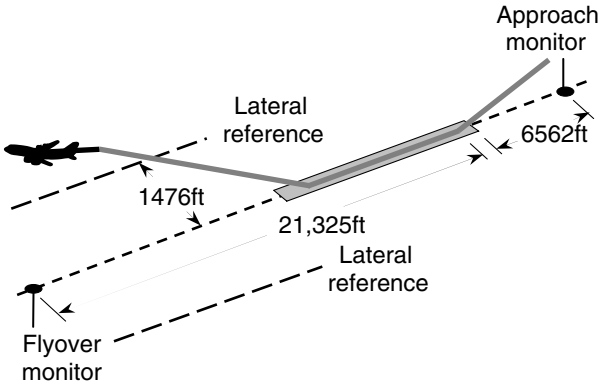

Fig. 5 Noise certification monitor arrangement relative to takeoff and landing flight paths.

of its maximum sea level static low-spool shaft speed (41,700 rpm). (A shaft speed of 96% was the highest engine power setting tested in the facility. Due to ambient temperature restrictions on the day of the test, 100% speed could not be achieved.) The spectrum is lossless and corrected for spreading to a 1 ft distance. Fan tones at the fundamental blade passage frequency (BPF) and its harmonics are identified in the figure. The fundamental fan tone is usually prominent, despite the cutoff fan design and the use of an inlet control device to eliminate inlet flow distortion. At most angles, another tone is present at the high-spool's shaft passage frequency (SPF_H). An additional prominent tone (with hay-stacking behavior) at much higher frequencies is created by the low-pressure turbine (LPT). When computing EPNL, regulations only consider noise up to the 10,000 Hz preferred one-third-octave band center frequency. Acoustic content above 11,220 Hz (the upper boundary frequency defined by the band filter required by ICAO) does not contribute to aircraft noise metrics. Thus, the 4 BPF fan tone only contributes to certification noise at lower shaft speeds or if Doppler effects in the aft quadrant are strong enough to shift it to lower frequencies. The strong turbine tone does not contribute to certification noise, even at lower engine power settings that would be used during approach. But because the turbine tone is so distinct from fan tones, the DGEN could be a useful research testbed for the study of turbine noise.

Perhaps the most expedient method for computing certification noise would be to use the measured engine spectra directly with a system noise analysis and propagation tool. Straightforwardly, the measured spectra could be analytically "flown" on a trajectory past observers on the ground. Propagation and ground effects could be applied and EPNLs computed for each observer. Convection and Doppler flight effects could be applied to improve accuracy.

However, there are problems with this approach. Engine behavior is different in flight than at ground level. Engine spool speeds, flow rates, temperatures, and pressures, all of which influence engine noise, vary with altitude and airspeed. Correcting these properties with referred temperature and pressure is helpful, but imperfect.

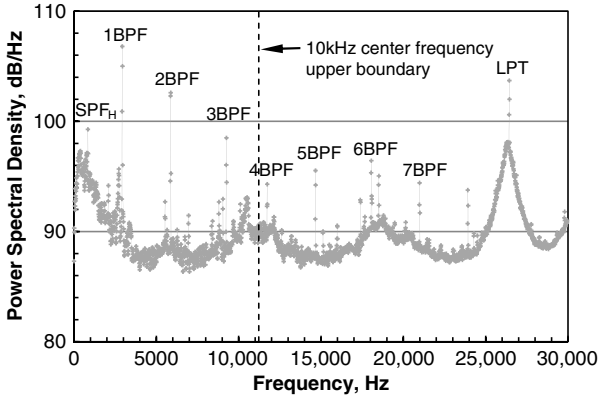

Fig. 6 DGEN turbofan power spectral densities at 118 deg from inlet axis, operating at 96% of maximum low-spool shaft speed.

Without additional rigor, noise measured statically on the ground is not wholly representative of noise in flight.

In addition, jet mixing noise is a distributed source radiating along the axial plume of the exhaust. The microphones in the NASA facility ranged from 32 to 57 ft away from the engine: distances far enough to be considered in the acoustic far field, but not sufficiently distant to treat the entire exhaust plume as a point source radiating from the nozzle. A technique is required to relate microphone geometric angles to the engine with apparent angles to jet noise source locations.

Instead, empirical source noise prediction methods are derived and are used in place of measured noise. Noise surrogate models are constructed as empirical functions of engine state variables such as spool speed, flow rate, temperature, and pressure. Empirical noise models are calibrated to the measured static spectra and they are relied on to project spectra to arbitrary flight conditions. Engine state data are obtained from Price Induction's Virtual Engine Test Bench: an engine performance simulator built around the DGEN's engine control unit. In this study, polynomial response surfaces are created for engine state properties throughout the engine as functions of altitude, flight Mach number, and low-pressure spool speed. This approach ensures that engine noise predictions react properly to changes in altitude and airspeed.

Using noise surrogate models in place of actual spectra allows for removal of extraneous or spurious portions of the spectra that are not believed to be genuine engine noise, particularly at low frequencies where the acoustic dome facility is not sufficiently anechoic. Further, if the engine noise sources are separated and modeled individually, each source can easily be manipulated mathematically. This is useful when simulating the effects of adding noise reduction technology such as duct acoustic treatment (which would be applied only to fan noise), nozzle chevrons (a jet noise reduction technology), or when conducting a noise uncertainty analysis of each component as it relates to the overall system. Last, component noise modeling allows for the removal of engine noise sources that may be eliminated or reduced during manufacturing and would not be present in the final production engine.

Engine noise modeling is discussed in detail in Sec. II.A. The measured spectra are corrected for atmospheric absorption. The levels of the lossless spectra can be adjusted to any distance using a spherical spreading correction (the actual distance to the microphone is used when developing the jet noise method so that distributed source effects can be modeled). Each noise method is formulated in the one-third-octave band paradigm, using decibels referenced to 20 μPa. When computing certification noise, convection and Doppler effects in each source noise model are applied and spectra are projected to flight conditions appropriate for a DGEN-powered airplane. A trajectory analysis is performed for a small notional personal light jet to determine the approximate flight path past each noise certification monitor. In-flight spectra are fed into NASA's Aircraft Noise Prediction Program as user-supplied noise, propagation losses and ground effects are applied, and certification noise levels are computed.

A. Engine Noise Sources

Core noise predictions are based on a simple empirical expression [8] suggested by the Society of Automotive Engineers. Lossless core noise spectra L_{Core} (in decibels, as a function of frequency f and polar emission angle θ) are expressed as a function of engine properties, namely, the mass flow rate entering the combustor, the change in total temperature through the combustor, and the density of the flow entering the combustor:

$$L_{\text{Core}}(f,\theta) = 10\log_{10}\left\{x_1 \frac{\dot{m}_{\text{Comb}}}{\dot{m}_{\text{Ref}}}\left[\frac{\Delta T_{\text{Comb}}}{T_{\text{Ref}}}\right]^2\left[\frac{\rho_{\text{Comb}}}{\rho_{\text{Ref}}}\right]^2 \frac{D(\theta)S(f,x_2)}{[1-M_f\cos\theta]^k}\right\} \tag{1}$$

The flow properties are rendered dimensionless with reference parameters. D is a dimensionless directivity function correcting levels for emission angle and S is a dimensionless function that accounts for spectral shaping and Doppler shift. In flight, levels are adjusted for

the flight Mach number M_f with the term $1 - M_f \cos\theta$ raised to a convective amplification exponent k (taken to be four for quadrupole emissions). The method defines core noise as direct and indirect unsteady combustion noise. Turbine noise is not included in the method, but in the DGEN engine, it is at such high frequencies that it is not expected to be relevant to certification noise. Spherical spreading and other propagation corrections are applied afterward.

The terms x_1 and x_2 are empirical calibration variables. Suggested values are given in the original reference and elsewhere, but in this study, they are variables intended to fit the predictive model (with $M_f = 0$) to the measured static spectra; x_1 adjusts core noise spectra for amplitude, whereas x_2 adjusts for curvature. Fitment of spectra is discussed in the following section.

Fan noise predictions are based on an early empirical method developed by NASA [9], but recalibrated for modern, wide-chord, low-pressure-ratio fans [10]. Acoustic power level is proportional to the mass flow rate entering the fan, the total temperature rise across the fan stage, and an empirical function dependent on the relative (helical) fan rotor tip Mach number. Lossless fan noise spectra L_{Fan} are given by

$$L_{\text{Fan}}(f,\theta) = 10\log_{10}\left\{x_3 \frac{\dot{m}_{\text{Fan}}}{\dot{m}_{\text{Ref}}}\left[\frac{\Delta T_{\text{Fan}}}{T_{\text{Ref}}}\right]^2 G(M_r)\frac{D(\theta)S(f,x_{4-8})}{[1 - M_f\cos\theta]^k}\right\} \tag{2}$$

The method models broadband and rotor–stator discrete interaction tones separately. In addition to accounting for Doppler shift, the spectral function S assigns an additional level representing an interaction tone whenever the one-third-octave frequency span contains a multiple of the blade passage frequency. In other implementations of the method, additional terms are present to account for effects such as variable rotor–stator spacing, inlet guide vanes, and flow distortion. These terms, however, are omitted here because they reduce to constants and because fan noise is already adjusted using the calibration variables x_3–x_8. In this instance, x_3 adjusts fan noise spectra for amplitude, x_4 adjusts for curvature, and x_5–x_8 adjust the levels of the first four interaction tones.

Shaft acoustic power is based on an empirical function H: a polynomial regression variable dependent on high and low spool shaft speeds. L_{Shafts} is given by

$$L_{\text{Shafts}}(f,\theta) = 10\log_{10}\left\{H(N_L,N_H)\frac{D(\theta)S(f,x_9,x_{10})}{[1 - M_f\cos\theta]^k}\right\} \tag{3}$$

The spectral function S assigns levels when the one-third-octave frequency span contains one or both shaft passage frequencies. It also accounts for Doppler shift. Finer adjustments to shaft order tone levels unaccounted for by H are made by x_9 and x_{10}.

Jet noise is modeled using a semi-empirical method developed by Stone et al. [11]. The problem is approached by breaking overall jet noise into several virtual components, each accounting for different noise-generation mechanisms within the jet plume. Because both the core and bypass nozzles are subcritical throughout the takeoff regime, the jets are modeled as shock-free streams, and shock-related jet noise components are ignored. Three turbulent mixing components are considered: 1) large-scale merged-stream mixing noise, 2) small-scale mixing noise, and 3) transitional intermediate-scale mixing noise. The general form of the three lossless mixing components is

$$L_{\text{Jet}}(f,\theta) = 10\log_{10}\left\{x_{11}(V_e/c_{\text{Ref}})^n(\rho/\rho_{\text{Ref}})^\omega \frac{D(\theta_e)S(f,\theta_e)}{(1 + M_c\cos\theta)^2 + \alpha^2 M_c^2}\right\} \tag{4}$$

where V_e is an effective jet velocity (normalized by ambient sound speed to form an acoustic Mach number), n is a velocity slope, ρ is a fully expanded jet density, and ω is a variable density exponent. Each represents an appropriate value for the jet noise component being considered. An effective polar emission angle dependent on jet velocity that accounts for refraction is given by θ_e. Although jet noise source locations vary, they are assumed to vary similarly with jet velocity and can be correlated to the geometric emission angle. Each spectrum is adjusted to the distance from the nozzle to the microphone before calibration (refraction modeling is discussed in greater detail in [11]). Stone et al. found that better agreement with in-flight data could be obtained by eliminating the convection term $1 - M_f\cos\theta$ and relying upon only a convective Mach number M_c and an empirical convection constant α to account for the effects of turbulent eddy decay. All three mixing noise components are summed and adjusted all at once by one calibration constant x_{11}.

B. Fitment of Spectra

A method is developed to calibrate the empirical noise models to the measured data. It is worth mentioning that calibrating the source noise models does not necessarily improve upon them in the general sense, but instead it simply makes them DGEN specific. This method of regression attempts to account for fitment of spectra as well as ensuring accurate representations of other derived noise metrics. A simple multivariable optimizer is used to aid fitment of the noise models to the measurements. A composite objective function $O(x)$ is defined as

$$O(\boldsymbol{x}) = w_1\frac{\sum_i (L_{i,\text{data}} - L_{i,\text{model}})^2}{\sum_i (L_{i,\text{data}} - \bar{L}_{\text{data}})^2} + w_2(L_{\text{TPN,data}} - L_{\text{TPN,model}})^2 \tag{5}$$

The first term is the residual sum of squares divided by the total sum of squares over all of the L_i sound pressure level observations of a spectrum. The first term, if driven to zero, would represent a perfect fit of noise models to the measured data, and it alone would suffice as an objective function. But neither the noise models nor the data are perfect representations of the system, and so obtaining a perfect fit is difficult. Further, at least as important as matching the spectral shape is matching the frequency-independent tone-corrected perceived noise level (PNLT, given the notation L_{TPN}), because it is the metric used directly to compute certification EPNL. Given this, the squared difference of L_{TPN} is added as a second term in $O(\boldsymbol{x})$. For each spectrum, the optimizer is allowed to vary the values of $\boldsymbol{x}$ within limits until $O(\boldsymbol{x})$ is minimized. Values for the weighting factors w_1 and w_2 are selected to drive the two terms in $O(\boldsymbol{x})$ to the same order of magnitude.

Of course, a minimum nonzero $O(\boldsymbol{x})$ does not result in a unique solution. Caution is warranted when using this logic to fit noise models. Generally, values of $\boldsymbol{x}$ should not stray too far from their nominal values. It is easy to envision a case, for example, where levels of one noise component are driven unrealistically high just to drive $O(\boldsymbol{x})$ a bit smaller, only to have a more realistic noise component overshadowed. Judicious limits should be set for values of $\boldsymbol{x}$, and graphical inspection of each calibrated spectrum is recommended. This is discussed in greater detail in Sec. III.

C. Airframe and Installation

Propulsion noise is combined with airframe noise appropriate for the notional airplane using the Fink method [12]. The method uses empirical functions to model noise spectra as functions of polar and azimuthal emission angles. Spectra are predicted for the trailing-edge planform surfaces, landing gear, and single-slotted flaps. The airplane is assumed to have fixed, nonretracting landing gear and no leading-edge slats. The method uses gross airframe dimensions such as span, flap chord lengths, and gear configuration and dimensions; all of which may be obtained from a simple open-literature, three-view aircraft drawing.

Noise shielding (also referred to as barrier attenuation or insertion loss) is an acoustic diffraction phenomenon where acoustic waves are attenuated when propagated past an impermeable barrier placed between the noise source and an observer. Shielding is particularly

efficient when the observer is located in the "shadow region" where the noise source is obscured. The wing planform provides a shielding surface for the engine located above and downstream of the wing trailing edge. Airframe noise sources and jet noise (a distributed source generated downstream throughout the axial exhaust plume) are not shielded.

The method used to predict shielding is a simple empirical diffraction model based on asymptotic results of optical diffraction theory, originally proposed by Maekawa [13] and reproduced in many foundational acoustic textbooks. The analytic treatment of diffraction effects in this manner is common in aeroacoustic applications. Reliable, fast, and easy to implement, it has been coded into aircraft noise system prediction programs.

Maekawa [13] proposed the shadow zone insertion loss relation

$$L_I = 20\log_{10}\left(\sqrt{2\pi|F|}/\tanh\sqrt{2\pi|F|}\right) + 5 \qquad (6)$$

in decibels, where F is the frequency-dependent Fresnel number $(2f\Delta/c)$, whose characteristic length Δ is the difference between the shortest path around the barrier between the source and the observer and the source–observer distance directly through the barrier. For observers in the bright zone ($F < -0.192$), the attenuation is neglected, and for observers in the transition zone ($-0.192 < F < 0$), it is appropriate to replace the hyperbolic tangent with the trigonometric tangent. Although the preceding relation is intended for use with semi-infinite barriers, Maekawa suggested that superposition may be used for barriers of finite length and width, such as a wing planform.

III. Results and Discussion

A. Spectral Results

The noise models are calibrated to every spectrum acquired in the facility. With 24 polar emission angles (ranging from 36 to 145 deg relative to the inlet axis) and six engine power settings (ranging from 47 to 96% of the maximum low-spool shaft speed), a dataset of 144 static spectra are available to perform a system noise assessment. Measured and modeled spectra at 138 deg and at the highest power setting are plotted in Fig. 7 for discussion. The sound pressure levels are lossless and referenced to a virtual observer on a 1 ft radius. The narrowband spectrum has a frequency interval of 12.2 Hz.

Tone content at the high-spool shaft frequency and at the first three fan passage frequencies are easily seen in the narrowband data. The narrowband data are summed to the one-third-octave band spectrum indicated by the symbols. Higher-frequency fan or turbine noise does not contribute to the analysis, because levels only at frequencies from 50 Hz to 10 kHz are used to compute noise certification metrics.

The calibrated spectra of fan, jet, core, and shaft noise models are also plotted. Fan and shaft noise levels are perhaps the easiest sources to identify and to calibrate. Both sources peak at frequencies where no other significant noise sources exist, and their prominent tones are easily identified and can be used as a guide. Fan noise sometimes required adjustments by as many as 8 dB relative to the levels predicted by the uncalibrated fan noise method of [10]. Tone content, incidentally, is anathema to applicants of noise-type certificates and to airplane occupants. In many cases, DGEN fan tones contribute strongly to the PNLT metric, owing primarily to the heavy tone correction penalty assigned to high-frequency tones. Acoustic treatment applied to the inlet and bypass ducts could abate these tones.

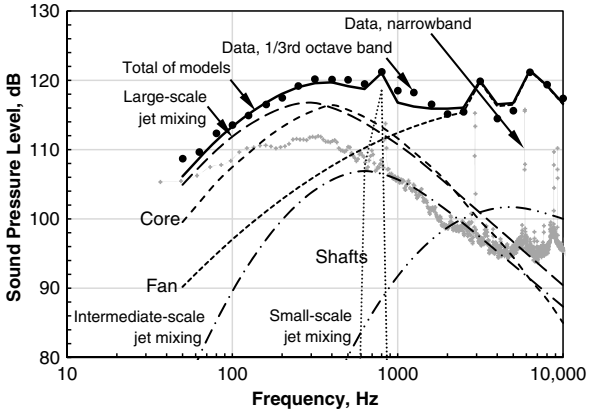

Fig. 7 Lossless spectra at 138 deg from inlet axis, 96% of maximum low-spool shaft speed, and referenced to a 1 ft distance.

From 50 to about 600 Hz, individual broadband noise sources are not as easily identified. At frequencies peaking at about 400 Hz, large-scale jet mixing noise and core noise coexist in some proportion. It is often difficult to tell when, or if, jet noise is masquerading as core noise or vice versa. One method to determine the contribution of core noise in a signal is to use source separation coherence techniques. During NASA's test of the DGEN engine, a semi-infinite tube transducer was mounted in the core tailpipe to measure pressure fluctuations in the exhaust. When an exhaust signal is analyzed along with signals from a companion microphone located in the far field, core noise can be reduced. Coherent combustor broadband noise was detected up to about 500 Hz using a two-signal coherent output power method [14]. Unfortunately, due to limits on time and resources, the tests were restricted to just one aft angle. Generally, the experiment revealed the core noise method of [8] to overpredict core noise by approximately 11 dB, requiring a large adjustment to the calibration variable x_1. Although this is a preliminary finding requiring further evaluation, it is helpful information when assigning values to jet and core noise calibration variables.

Another technique is to use lower engine throttle settings as a guide in setting core noise calibration variables. At low engine power, jet velocity (and jet noise) is quite low, and so the presumption is that core noise is the most prominent low-frequency feature in the spectra. As engine power is increased and jet noise level rises (indeed, very dramatically, with velocity to the eighth power), the physics-based source noise models are relied on to report the correct proportions of jet versus core noise. Both the source separation experiment result and low-power-setting data are used as guides in calibrating jet and core noise models.

In general, jet noise predictions are adjusted little (usually by less than 1 dB), whereas core noise predictions are reduced. Still, without more rigor in separating core and jet noise, the results are lumped together when reporting component contributions to the certification noise level.

B. Airplane Trajectory

Airplane trajectories and engine operating conditions have an important influence on certification noise. Airplane takeoff and landing trajectories are computed using an aircraft trajectory simulation tool. Engine thrust data collected from the DGEN digital control system and aerodynamics representative of a general aviation airplane are inputs to the trajectory analysis.

Trajectory data evaluated for a sea level field at 77°F are shown in Fig. 8. Altitude above field elevation, true airspeed, and true thrust per engine are plotted against the distance from brake release. The trajectories are shown with takeoff and landing operations superimposed. For presentation purposes, the touchdown point on landing is coincident with the point of brake release on takeoff. Thrust for the noise abatement engine power cutback is set such that the climb gradient is zero with one engine inoperative, or 4% with both engines operating. It is completed at approximately 17,000 ft from brake release. On approach, a 3 deg glide slope is followed, the maximum landing weight is assumed, and the single-slotted flaps are extended. The engine thrust is set to a level that maintains a stable glide slope.

The triangular markers on each chart denote noise certification measurement locations. The approach microphone markers in Fig. 8 are 6562 ft behind the runway threshold and approximately 7518 ft behind the instrument landing system touchdown zone on the runway centerline. The monitor is located under the point of the approach path where the airplane is 394 ft above ground level. The lateral microphone location lies along a sideline parallel to the runway, displaced 1476 ft from the extended runway centerline. It is located

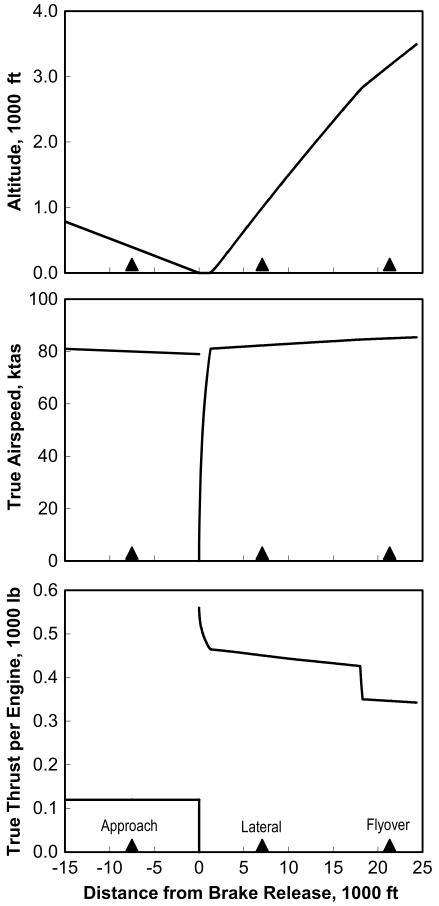

Fig. 8 Departure and arrival trajectories.

along the sideline across from the location where the airplane reaches an altitude of 1000 ft above field elevation (i.e., the point where ground attenuation effects diminish and where maximum lateral noise is typically observed). The flyover microphone markers in Fig. 8 are 21,325 ft from brake release on the extended runway centerline.

C. Noise Certification Results

Flight conditions and engine power settings are used as inputs to the calibrated noise models for each certification noise prediction. Static component noise spectra are projected to flight conditions, summed in the vicinity of the airplane, and propagated to the ground using the ANOPP software. EPNLs at each observation station are determined from PNLT versus time histories at 0.5 s time intervals. Component and total system EPNLs are shown in Fig. 9. The effect of shielding is shown in the rightmost columns. Jet and core noise levels are not reported individually due to the spectral separation issues described earlier.

Fan noise dominates the approach and, to a lesser degree, lateral noise signatures. Jet and core noise dominate flyover noise and contribute to lateral noise. Shaft noise appears to play a minor role in lateral and flyover noise levels, but not at approach. Even if shaft noise sources could be identified and addressed during engine production, it would not significantly reduce certification noise. Airframe sources, even when taken together, contribute only a few tenths of an EPNdB to the approach level. Wing planform shielding effects (applied to fan, core, and shaft noise) reduce EPNL by 1.7, 0.9, and 0.7 EPNdB at the approach, lateral, and flyover locations, respectively.

Predicted noise levels of the notional DGEN 380 twinjet are plotted against maximum takeoff gross weight in Fig. 10. The error bands surrounding the predictions represent one standard deviation of uncertainty determined by a Monte Carlo experiment discussed in the next section. Chapter 3 limits are shown for each certification location, and the anticipated Chapter 14 limit for twinjets is shown in

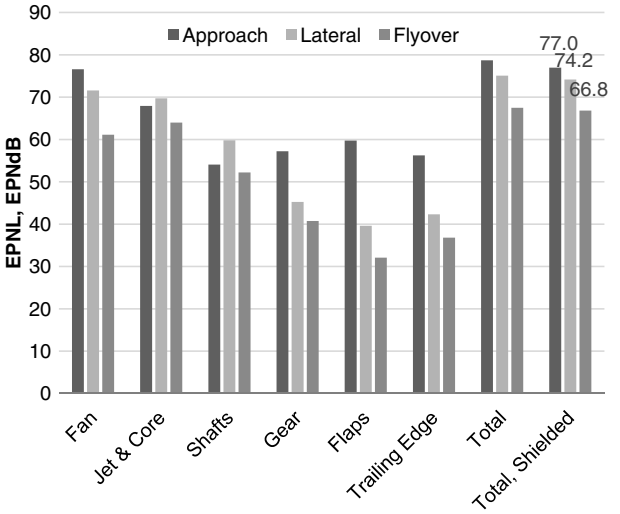

Fig. 9 EPNL predictions.

the cumulative chart. Chapter 14 limits for aircraft of this size (under 55,000 kg) are expected to debut on 31 December 2020. The predictions are also compared against published EPNLs of other aircraft.[‡]

D. Uncertainty Analysis

Because the results are determined from a variety of largely unknown elements, a Monte Carlo uncertainty analysis is performed to provide insight into the system model. Normally deterministic, the benchmark noise model is transformed into a stochastic model by replacing portions of its input data with continuous random values. A vector of input variables representing modeling unknowns is randomly permuted using probability distributions centered around the model's nominal values. The input variables subject to randomization are chosen by a top-down decomposition of the system noise problem.

These uncertainty variables are presented in Table 1. The variables are chosen to represent various effects that would certainly stray from median values assumed for the benchmark case during the course of aircraft development. Randomly changing variables represent the lack of knowledge of system characteristics, as well as the accuracy of (and uncertainty in) source noise prediction methods. Notably, atmospheric properties are not varied, despite their strong influence on atmospheric absorption and other phenomena. Because ICAO requires acoustic measurements to be corrected to standard acoustic day conditions, there is little reason to include ambient temperature or relative humidity in the experiment. There are no variables assigned to represent variations in wind, terrain, or airport elevation for similar reasons.

Because the airplane is notional, all trajectory-related variables are subject to variability. Engine power settings on approach and during the noise abatement thrust cutback are dependent on airplane weight, aerodynamics, and regulations. These variables are allowed to change within limits judged reasonable using triangular distribution models. Also, each noise source is allowed to vary by adding or subtracting uncertainties in decibels. In other words, for every sample in the Monte Carlo experiment, the frequency- and angle-dependent spectra predicted by the calibrated source noise models are adjusted by simple constants (independent of frequency and emission angle) determined by normal probability distributions. The adjusted sources are summed in the vicinity of the airplane before propagation. Propulsion noise uncertainties are thought to be not usually more than measurement error and are assigned a standard deviation of just 1.0 dB. Airframe noise sources are assigned somewhat more variability than propulsion sources because the airplane configuration is

[‡]Data available online at www.easa.europa.eu/document-library/noise-type-certificates-approved-noise-levels [retrieved March 2015].

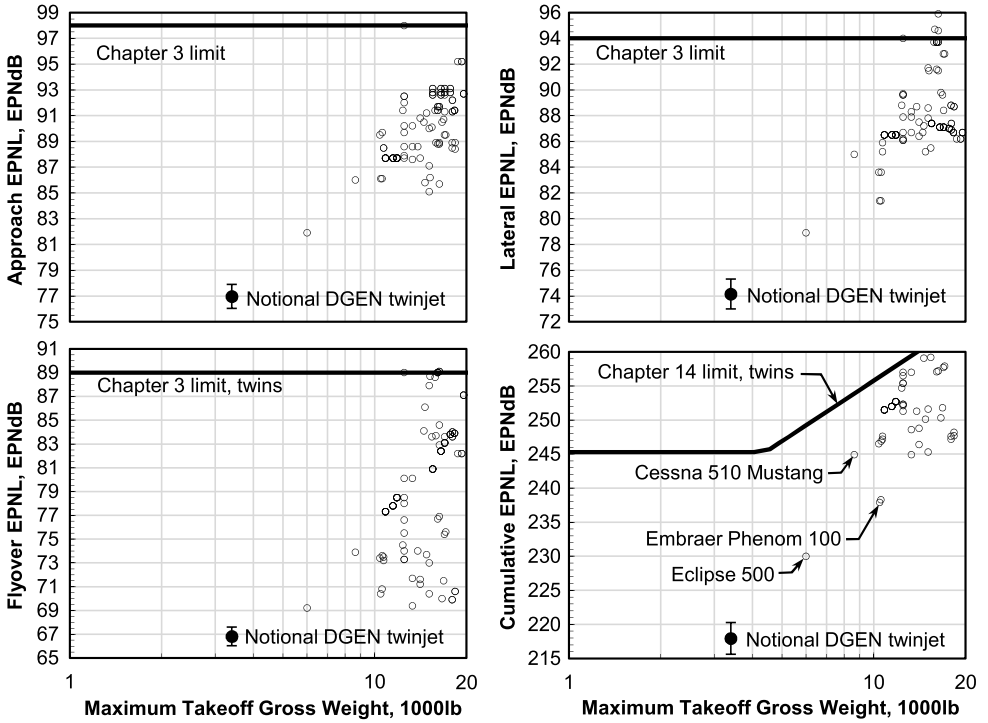

Fig. 10 Notional DGEN twinjet noise predictions compared with certification data and Chapter 3 and 14 limits. Error bars represent one standard deviation in an uncertainty analysis.

not precisely known. Further, ground-specific flow resistance and lateral attenuation are environmental variables affecting noise during certification testing. Last, the wing planform shielding area is allowed to vary uniformly from zero (no shielding) to a maximum of 200 ft^2. As wing area is varied, wing aspect ratio, taper ratio, and sweep are held constant.

The three certification EPNLs comprise the set of stochastic output response variables. A single analysis requires about 3 min to execute on a contemporary office computer. The Monte Carlo problem lends itself to concurrent parallelization, and so the analyses may be multithreaded across several platforms. A robot is easily constructed to modify a template input file, permute its contents with randomly generated inputs, and run the analysis. The noise model is interrogated 8000 times. Results of the uncertainty experiment are shown in Fig. 11 for cumulative EPNL. Statistics for the experiment are presented in Table 2.

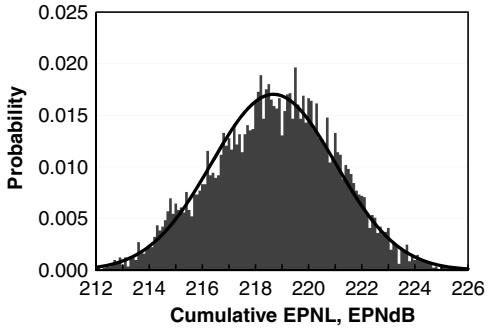

Fig. 11 Monte Carlo uncertainty analysis of cumulative EPNL. Histogram and normal distribution generated from 8000 samples and bin span of 0.1 EPNdB.

Table 1 Uncertainty variables used in Monte Carlo experiment

Variable	Median	Model	Minimum	Maximum	Standard deviation
Approach flight Mach no.	0.119	Triangular	0.112	0.126	— —
Lateral flight Mach no.	0.123	Triangular	0.119	0.127	— —
Flyover flight Mach no.	0.128	Triangular	0.120	0.150	— —
Approach N_L setpoint	60%	Triangular	58%	62%	— —
Lateral N_L setpoint	96%	Triangular	94%	100%	— —
Flyover N_L setpoint	90%	Triangular	87%	93%	— —
Approach angle of attack	6 deg	Triangular	5 deg	7 deg	— —
Lateral angle of attack	6 deg	Triangular	5 deg	7 deg	— —
Flyover angle of attack	6 deg	Triangular	5 deg	7 deg	— —
Flyover altitude	3170 ft	Triangular	2850 ft	3490 ft	— —
Fan noise adjustment	0	Normal	— —	— —	1.0 dB
Core noise adjustment	0	Normal	— —	— —	1.0 dB
Shaft noise adjustment	0	Normal	— —	— —	1.0 dB
Jet noise adjustment	0	Normal	— —	— —	1.0 dB
Landing gear noise adjustment	0	Normal	— —	— —	1.0 dB
Flap noise adjustment	0	Normal	— —	— —	1.0 dB
Trailing-edge noise adjustment	0	Normal	— —	— —	1.0 dB
Ground-specific flow resistance	291 sl/s-ft^3	Triangular	233 sl/s-ft^3	349 sl/s-ft^3	— —
Lateral attenuation adjustment	0	Triangular	−2 dB	2 dB	— —
Wing area (shielding)	155 ft^2	Uniform	0	200 ft^2	— —

Table 2 Uncertainty statistics in EPNdB

Statistic	Approach	Lateral	Flyover	Cumulative
Benchmark case	77.0	74.2	66.8	217.9
Minimum of samples	74.3	70.6	64.4	209.5
Maximum of samples	80.5	78.1	69.7	226.4
Range of samples	6.2	7.6	5.3	17.0
Mean of samples	77.3	74.6	66.8	218.7
Standard deviation	0.9	1.2	0.8	2.3

After 8000 samples, there do not appear to be multiple modes or truncations in any of the histograms. Skew and kurtosis are not major factors. As is the case in any uncertainty experiment, the spread of the data perhaps is the most revealing. The standard deviations are rather small, on the order of only 1 EPNdB at each observer.

IV. Conclusions

Static noise measurements of a DGEN 380 turbofan are used to develop propulsion noise prediction models. The models are calibrated to measured data using a process that fits them not only to the shape of each experimental spectrum, but also to other derived noise metrics of importance. Embedded physics-based behavior allows the models to react properly to changing engine state and flight conditions. The calibrated noise models are used to analytically project noise spectra to flight conditions and to predict system noise of a notional airplane powered by twin DGEN engines. A Monte Carlo experiment is used to compute uncertainty in the system noise results.

Acknowledgment

This work was performed with support from NASA's Advanced Air Transport Technology Project.

References

[1] "Environmental Technical Manual, Vol. I, Procedures for the Noise Certification of Aircraft," *International Civil Aviation Organization (ICAO), Committee on Aviation Environmental Protection*, 2nd ed., Document 9501, 2015, pp. 4.69–4.83.

[2] Herkes, W. H., and Reed, D. H., "Modular Engine Noise Component Prediction System (MCP) Technical Description and Assessment Document," NASA CR-2005-213526, 2005.

[3] IHS Jane's Information Group, "Engineering Sciences Data Unit series on Aircraft Noise (www.esdu.com)," *Aircraft Engineering and Aerospace Technology*, Vol. 70, No. 4, 1998.

[4] Gillian, R. E., "Aircraft Noise Prediction Program User's Manual," NASA TM-84486, 1983.

[5] Zorumski, W. E., "Aircraft Noise Prediction Program Theoretical Manual, Parts 1 and 2," NASA TM-83199, 1982.

[6] "Annex 16 to the Convention on International Civil Aviation, Vol. I: Aircraft Noise," *International Standards, and Recommended Practices—Environmental Protection*, 7th ed., International Civil Aviation Organization, Montreal, July 2014.

[7] "Noise Standards: Aircraft Type and Airworthiness Certification," U.S. Code of Federal Regulations, Federal Aviation Advisory Circular 36-4C, 2003, Title 14, Chap. 1, Part 36.

[8] Emmerling, J. J., Kazin, S. B., and Matta, R. K., "Core Engine Noise Control Program. Vol. III, Supplement 1—Prediction Methods," FAA RD-74-125, III-I, March 1976.

[9] Heidmann, M. F., "Interim Prediction Method for Fan and Compressor Source Noise," NASA TMX-71763, 1979.

[10] Krejsa, E. A., and Stone, J. R., "Enhanced Fan Noise Modeling for Turbofan Engines," NASA CR-2014-218421, 2014.

[11] Stone, J. R., Krejsa, E. A., Clark, B. J., and Berton, J. J., "Jet Noise Modeling for Suppressed and Unsuppressed Aircraft in Simulated Flight," NASA TM-2009-215524, 2009.

[12] Fink, M. R., "Airframe Noise Prediction Method," FAA RD-77-29, March 1977.

[13] Maekawa, Z., "Noise Reduction By Screens," *Memoirs of the Faculty of Engineering*, Vol. 12, Kobe Univ., Kobe, Japan, 1966, pp. 472–479.

[14] Bendat, J. S., and Piersol, A. G., *Engineering Applications of Correlation and Spectral Analysis*, Wiley-Interscience, New York, 1980.